Pergamon

Int. J. Heat Mass Transfer. Vol. 38, No. 11, pp. 2039–2046, 1995

0017-9310/95 $9.50 + 0.00

0017-9310(94)00318-1

Effects of multiple obstructions on natural convection heat transfer in vertical channels

PRASAD VISWATMULA and M. RUHUL AMIN†

Department of Mechanical Engineering, Montana State University, Bozeman, MT 59717, U.S.A.

(*Received* 8 *July* 1993 *and in final form* 22 *September* 1994)

Abstract—Free convection flows in vertical channels with two rectangular obstructions on opposite walls was studied numerically. Four different geometries were employed to study the effect of the parameters like Rayleigh number (*Ra*), aspect ratio (*Ar*), and obstruction locations (L_1, L_2) on the average Nusselt number (*Nu*). The results included isotherms, streamlines and Nusselt numbers. Average Nusselt numbers for the obstructed channels were less than those of the smooth channel. The maximum reduction in heat transfer found in this study is approximately 31% and occurred at $Ra = 5 \times 10^2$. The minimum reduction in heat transfer is approximately 3% and occurred at $Ra = 10^4$.

1. INTRODUCTION

Laminar free convection has many engineering applications. Some of these applications are the cooling of electronic equipment, solar collection systems, building energy systems, and fin-tube baseboard heaters. Among these, cooling of electronic equipment draws much attention because of the microminiaturization (which results in higher functional and power densities) and the use of semi-conductor devices which require fairly close temperature control. The vertical channel flow configuration is of primary interest in most electronic equipment applications. The component cards are assembled in vertical or inclined arrays, with small gaps or channels between each card. The inlet and exit of the these channels are open to the ambient conditions. Repeating cross-sectional protuberances or flow restrictions on the surface of a vertical channel are a common occurrence. The flow found in blocked passages of vertical channels or ducts of small dimensions is in a developing regime. The effect of obstructions on heat transfer in such channels draws special attention.

Considerable analytical and experimental investigations were done on free convection between parallel plates [1–4]. Anand *et al.* [5] studied numerically the effect of plate spacing on free convection between vertical parallel plates. Levy [6] derived the optimum plate spacings for laminar natural convection heat transfer from parallel vertical isothermal flat plates. In another study, experimental verification of this optimum plate spacing was done by Levy *et al.* [7]. Wirtz and Stutzman [8] studied experimentally the free convection of air between parallel plates with symmetric heating. Aung [9] analyzed and presented, in closed forms, the fully developed solutions for laminar free convection in a vertical, parallel plate channel with asymmetric heating. Aung *et al.* [10] investigated numerically as well as experimentally the developing laminar free convection between vertical flat plates with asymmetric heating.

Webb and Hill [11] conducted experiments on high Rayleigh number laminar natural convection in an asymmetrically heated vertical channel. Carpenter *et al.* [12] investigated numerically the interaction of radiation and free convection between vertical flat plates with asymmetric heating. Cha *et al.* [13] used a finite difference numerical method to simulate natural convection between two vertical parallel plates where one plate was subjected to oscillating surface temperature boundary condition.

Kim and Boehm [14] investigated numerically the combined free and forced convective heat transfer from multiple rectangular wall blocks in vertical channels. Studies on mixed and natural convection in channels with single obstruction can be found in refs. [15–17]. Mehrotra and Acharya [18] conducted an experimental study of natural convection heat transfer in smooth and ribbed UWT and UHF vertical channels.

From the above discussion, it can be seen that there is a necessity to study the compound effect of (i) multiple obstructions, (ii) obstructions on both walls of the channel, (iii) aspect ratio of channel and (iv) location of the obstruction. The present numerical study is aimed at studying the effect of the aforesaid factors on the rate of heat transfer.

†Author to whom correspondence should be addressed.

NOMENCLATURE

Ar	aspect ratio of the channel ($= b/L$)
b	channel width
C_p	specific heat of fluid
g	acceleration due to gravity
$\bar{h}$	thickness of the obstruction
h	dimensionless thickness of the obstruction, $\bar{h}/L$
k	fluid thermal conductivity
L	channel height
$\bar{L}_1$	height of the obstruction on the left wall from the channel entrance
$\bar{L}_2$	height of the obstruction on the right wall from the channel entrance
L_1	dimensionless height of the obstruction on the left wall from channel entrance, $\bar{L}_1/L$
L_2	dimensionless height of the obstruction on the right wall from channel entrance, $\bar{L}_2/L$
Nu	average Nusselt number
Nu_y	local Nusselt number
p	ambient pressure
p_∞	static pressure
P	dimensionless pressure, $[p-p_\infty]/[g\beta\rho_\infty\Delta TL]$
Pr	Prandtl number, $\mu C_p/k$
Ra	Rayleigh number, $g\beta\Delta Tb^3/\alpha\nu$
$\bar{T}$	fluid temperature
T_w	wall temperature
T_∞	ambient temperature
T_f	average film temperature, $[T_w+T_\infty]/2$
ΔT	(T_w-T_∞)
$\bar{u}$	$\bar{x}$-component of velocity
$\bar{v}$	$\bar{y}$-component of velocity
u	dimensionless x-component of velocity, $\bar{u}b/\alpha$
v	dimensionless y-component of velocity, $\bar{v}b^2/\alpha L$
$\bar{x}$	Cartesian x-coordinate
$\bar{y}$	Cartesian y-coordinate
x	dimensionless x-coordinate, $\bar{x}/L$
y	dimensionless y-coordinate, $\bar{y}/L$.

Greek symbols

α	thermal diffusivity
β	thermal expansion coefficient of fluid
ε	tolerance parameter
μ	dynamic viscosity of fluid
θ	dimensionless temperature for UWT, $[\bar{T}-T_\infty]/[T_w-T_\infty]$
ν	kinematic viscosity of fluid
ρ	density of fluid.

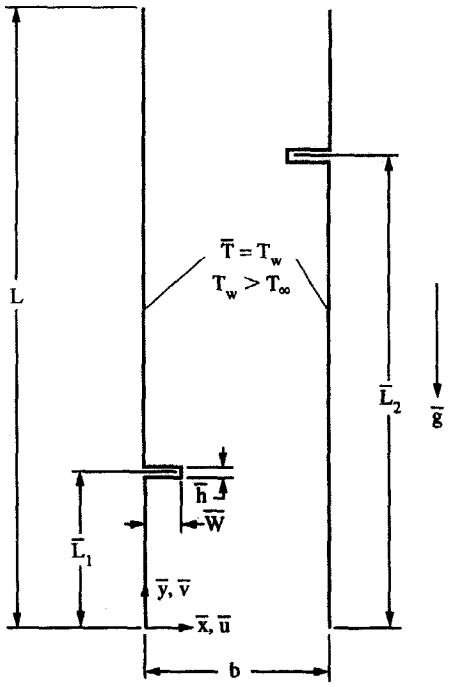

Fig. 1. Geometry of the obstructed channel.

2. PROBLEM FORMULATION

The governing equations for the flow in a vertical channel are parabolic in nature. But the presence of obstructions makes these governing equations elliptic. Also, the momentum and energy equations are coupled and therefore need to be solved simultaneously. Besides being elliptic and coupled, the partial differential equations are also non-linear. In the present study, the free convection flows of interest for a Newtonian fluid with no internal heat generation are assumed to be laminar, steady-state, two-dimensional and with constant properties. The fluid is assumed to be incompressible, with one exception. This exception is to account for the effect of variable density in buoyancy force (known as the Boussinesq approximation). Other valid assumptions are that the viscous dissipation, compressible work, and radiative transport are negligibly small. Geometry of the obstructed channel is shown in the Fig. 1. With these assumptions, the basic conservation equations can be written in nondimensional form as follows. Conservation of mass:

$$\frac{\partial u}{\partial x}+\frac{\partial v}{\partial y}=0. \tag{1}$$

Conservation of momentum:

$$\left(\frac{Ar^2}{Pr}\right)\left[u\frac{\partial u}{\partial x}+v\frac{\partial u}{\partial y}\right] = -(RaAr)\frac{\partial P}{\partial x}+Ar^2\left[\frac{\partial^2 u}{\partial x^2}+Ar^2\frac{\partial^2 u}{\partial y^2}\right] \quad (2)$$

$$\left(\frac{1}{Pr}\right)\left[u\frac{\partial v}{\partial x}+v\frac{\partial v}{\partial y}\right] = (RaAr)\left(\theta-\frac{\partial P}{\partial y}\right)+\left[\frac{\partial^2 v}{\partial x^2}+Ar^2\frac{\partial^2 v}{\partial y^2}\right]. \quad (3)$$

Conservation of energy:

$$u\frac{\partial \theta}{\partial x}+v\frac{\partial \theta}{\partial y}=\frac{\partial^2 \theta}{\partial x^2}+Ar^2\frac{\partial^2 \theta}{\partial y^2}. \quad (4)$$

The nondimensional boundary conditions for the above equations can be expressed as:

$$u = v = 0 \text{ and } \theta = 1 \text{ on left and right walls} \quad (5)$$

$$\left\{\begin{array}{c} u=0 \\ -P+\left(\frac{Ar}{Ra}\right)\frac{\partial v}{\partial y}=0 \\ \frac{\partial \theta}{\partial y}=0 \end{array}\right\} \text{ for } 0 \leqslant x \leqslant 1 \text{ and } y = 1 \quad (6)$$

$$\left\{\begin{array}{c} u=0 \\ -P+\left(\frac{Ar}{Ra}\right)\frac{\partial v}{\partial y}=0 \\ \theta=0 \end{array}\right\} \text{ for } 0 \leqslant x \leqslant 1 \text{ and } y = 0. \quad (7)$$

It is worth mentioning here that the elemental surface integrals generated by the Galerkin method of weighted residuals (GMWR) vanish. For the present study, the two natural (or Neumann) boundary conditions, i.e. the total stress normal to the boundary and the heat flux normal to the boundary are naturally enforced (known as 'weak enforcement') through the elemental surface integrals.

3. NUMERICAL INVESTIGATION

The finite element code NACHOS II was used to solve the governing equations. Detailed description of the code can be found in the refs. [19] and [20]. This code is a general purpose program developed for the solution of two-dimensional, viscous, incompressible fluid dynamics problems. The Galerkin method of weighted residuals (GMWR) is used in the code to discretize the partial differential equations. Apart from the numerical aspects, two features of any natural convection problem that must be paid attention are: (i) validity limits of the Boussinesq approximation, and (ii) selection of a reference temperature to take care of the variable property effects.

As suggested by Zhong *et al.* [21], the difference between the wall and ambient temperature was chosen so that $[T_w - T_\infty]/T_\infty \leqslant 0.1$ (or the driving force, $\beta\Delta T \leqslant 0.1$). The results of any fluid flow problem (with the fluid properties being temperature dependent) depend on the selection of a proper reference temperature. Film temperature with $\beta = 1/T_\infty$ was used as the reference temperature [22].

For the smooth as well as the obstructed channel, different aspect ratios were obtained by changing the distance, b, between channel walls. A smooth channel was used to study the effect of the obstructions on the vertical walls. A new mesh was developed for each aspect ratio of the channel. Aspect ratios of 0.2 and 0.3 were used for both the smooth and obstructed channels. More elements were packed in the regions of large temperature and/or velocity gradients. This yielded non-uniform mesh in all the cases.

To test the grid-independency, two different non-uniform meshes were used for the smooth channel with $Ar = 0.2$. Initially, a mesh of 250 subparametric, nine node, quadrilateral elements were used and then the elements were increased to 420 (an increase of 68%). The computed average Nusselt numbers in both the cases agreed very well with each other, with a maximum difference of 2%. Based on this comparison and the fact that the central processing unit (C.P.U) time required to run a particular case is in direct proportion to the number of elements in the mesh, a grid size of 250 elements was used. NACHOS II calculates the maximum elemental mass balance error for the numerical grid and it was observed that this error was of the order of 10^{-6} for all the cases. In addition, mass conservation was verified numerically by considering the inlet and the exit of the channel and it was found to be satisfied within a percentage difference of 1%.

The results of the grid independency test for the smooth channel were used as a base to decide the grid size for the obstructed channels. That is, the grid spacings for all the subsequent cases were chosen such that it was proportional to the grid spacing of the base case of the smooth channel. For convergence criteria, NACHOS II uses the discrete norms defined by

$$d^U_{n+1} = \frac{1}{U_{max}}\left[\sum_{j=1}^{N}(U_j^{n+1}-U_j^n)^2\right]^{1/2}$$

$$d^T_{U+1} = \frac{1}{T_{max}}\left[\sum_{j=1}^{N}(T_j^{n+1}-T_j^n)^2\right]^{1/2}. \quad (8)$$

In equation (8), the subscript max indicates the maximum value of the variable found at the $(n+1)$th iteration, and N is the total number of nodal points. For convergence, the following inequalities were satisfied

$$d^U_{n+1} \leqslant \varepsilon^U \text{ and } d^T_{n+1} \leqslant \varepsilon^T \quad (9)$$

where ε, the tolerance parameter, was set to be 10^{-3}.

The normalized equations and the boundary conditions discussed earlier indicate that the parametric study of the present problem involves the parameters Ra, Ar, L_1, L_2, W and h. A total of 30 cases corresponding to two aspect ratios ($Ar = 0.2, 0.3$) were run for the smooth channel. Average Nusselt numbers were calculated for all these cases so that they could be used as the standard of comparison for the obstructed channels.

For the obstructed channel, two aspect ratios ($Ar = 0.2, 0.3$) were used. For each aspect ratio, two sets of values for L_1 and L_2 were used to define the locations of the obstructions on the vertical walls. The sets of values used for L_1 and L_2 were (i) $L_1 = 0.25$, $L_2 = 0.75$, (ii) $L_1 = 0.5$, $L_2 = 0.5$. These values of L_1 and L_2 and the two different values of the aspect ratio resulted in four different geometries for the obstructed channel. These geometries are defined below.

Geometry I: $Ar = 0.2, L_1 = 0.25, L_2 = 0.75$;
Geometry II: $Ar = 0.2, L_1 = 0.5, L_2 = 0.5$;
Geometry III: $Ar = 0.3, L_1 = 0.25, L_2 = 0.75$;
Geometry IV: $Ar = 0.3, L_1 = 0.5, L_2 = 0.5$.

The range of Rayleigh number used in this study was $10^2 \leqslant Ra \leqslant 5 \times 10^4$. The values for W and h (define the size of the obstruction) were kept constant with $W = 0.0667$ and $h = 0.01334$. This was done to minimize the number of parameters varied and as such reduce the size of the computational matrix. Based on these criteria, 54 cases were run for the channel with obstruction. The detailed computational matrix is documented in ref. [23].

4. RESULTS AND DISCUSSION

Figure 2 shows the computed streamlines and isotherms for geometry I ($Ar = 0.2$) at $Ra = 10^2$ and 10^4. The following observations can be made from this figure.

(a) From the isotherm plots, it can be seen that at low Rayleigh numbers (e.g. $Ra = 10^2$), all the heat transfer takes place near the entrance region of the channel. In other words, beyond the channel entrance, the fluid temperature approaches that of the wall temperature and as such no heat transfer. In contrast, at high Rayleigh numbers (e.g. $Ra \geqslant 5 \times 10^3$), the heat transfer takes place throughout the channel length.

(b) It can also be observed that at higher values of Ra, large temperature gradients exist near the tip of the lower obstruction ($L_1 = 0.25$) as compared to the upper obstruction ($L_2 = 0.75$).

(c) For the range of Rayleigh numbers investigated, it can be observed that the density of the streamlines increases (i.e. the fluid velocity increases) in the regions around the tips of the obstructions. This is due to (i) reduction in the cross-sectional area of the channel around the tips of the obstructions, (ii) velocity magnitude is proportional to the stream function gradient, and also (iii) the boundary layer thickness is relatively small in the frontal side and particularly around the lower, outside corner of the obstruction.

(d) As the fluid approaches and passes over the obstructions, it undergoes a sequence of deceleration and acceleration. The boundary layer thickness is affected by this series of low and high velocity regions. The boundary layer thickens considerably in the regions above and below the obstruction and this leads to the recirculating zones above and below the obstructions.

(e) The recirculating zones below the obstructions are usually quite small and difficult to plot. However, a small recirculating zone above the upper obstruction is detected at higher Rayleigh numbers, and is shown in Fig. 2(c).

In order to study the effect of the obstruction on the rate of heat transfer, local Nusselt numbers (Nu_y) along the right wall are plotted against the elevation in the channel (i.e. y/L) and are shown in Fig. 3. It is seen from this figure that the lowest values of local Nusselt numbers are at the two intersections between the obstruction and the wall. The local Nusselt number (Nu_y) then increases to a pick value at the lower, outside corner (or tip, e.g. point 3 in Fig. 3) of the obstruction. As mentioned earlier, the velocity of the fluid increases near the tip of the obstruction and leads to an increase in the local heat transfer coefficient to a maximum value. The reduction in heat transfer rates at points 2 and 5 in the figure is due to the presence of stagnant fluid and recirculation flow. A similar trend was observed for local Nusselt number on the left wall of the channel.

Figure 4 shows the computed streamlines and isotherms for geometry II ($Ar = 0.2$). These are symmetric about the vertical axis of the channel. The observations (a), (c), (d) and (e) for the previous geometry are also true for this geometry. As can be seen in Fig. 4, two relatively large recirculation zones are formed just above the obstructions at higher values of Rayleigh numbers. The effect of these recirculating zones on heat transfer is discussed later. The two obstructions for this geometry are facing each other and reduce the flow cross-sectional area by nearly 67%. This leads to an increased velocity for heat transfer in this region. The distribution of local Nusselt numbers along the channel walls for this geometry was found to be of the same nature as geometry I (Fig. 3).

In order to study the effect of multiple obstructions on the heat transfer rate, the computed average Nusselt numbers from the numerical solutions of both obstructed and unobstructed channels are plotted against the Rayleigh number, Ra. This comparison is shown in Fig. 5. The average Nusselt numbers for geometry I are higher than those of geometry II. By comparing with the curve corresponding to the smooth channel, it is clear from this figure that obstructions reduce the heat transfer rate. To deter-

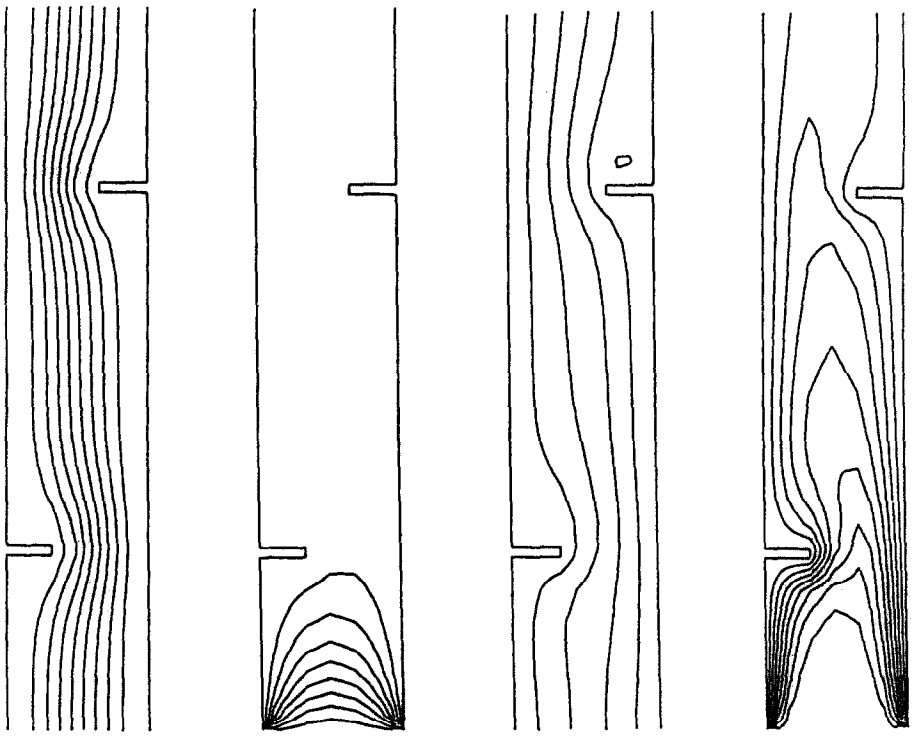

(a) Streamlines Ra = 10^2 (b) Isotherms Ra = 10^4 (c) Streamlines Ra = 10^2 (d) Isotherms Ra = 10^4

Fig. 2. Computed streamlines and isotherms for geometry I.

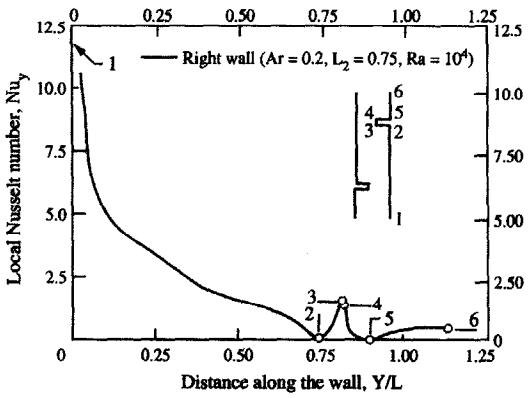

Fig. 3. Local Nusselt number distribution along the right wall for geometry I with $Ra = 10^4$.

mine the amount of reduction in heat transfer due to obstructions, ratios of the average Nusselt numbers of the obstructed to smooth channels were calculated at different Rayleigh numbers. It was found that at any particular Rayleigh number, the percent reduction was more for geometry II than for geometry I. The maximum reduction in heat transfer for geometry I was approximately 16% and occurred at a Rayleigh number of 5×10^2. The minimum reduction for geometry I was approximately 5% and occurred at the highest Rayleigh number, i.e. $Ra = 5 \times 10^4$. For geometry II, the maximum reduction in heat transfer

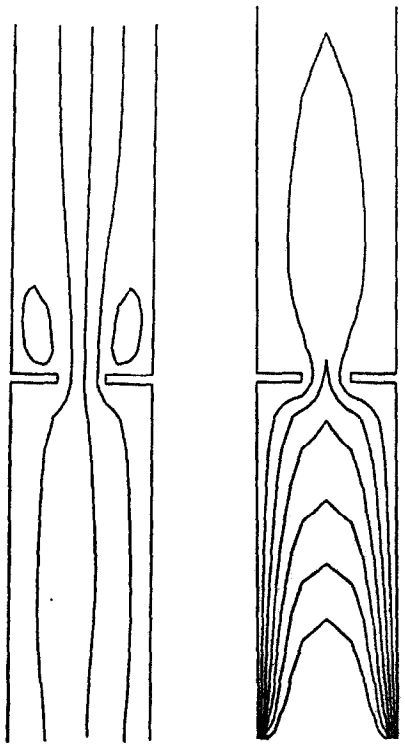

(a) Streamlines (b) Isotherms

Fig. 4. Computed streamlines and isotherms for geometry II with $Ra = 10^4$.

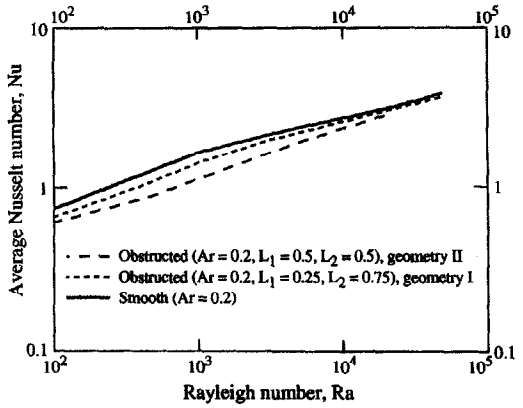

Fig. 5. Comparison of the average Nusselt numbers for the obstructed and unobstructed channels with $Ar = 0.2$.

was approximately 31% at $Ra = 5 \times 10^2$, and the minimum reduction in heat transfer was approximately 7.5% at $Ra = 2 \times 10^4$.

The above reduction in heat transfer can be explained from the streamline plots of Figs. 2(c) and 4(a). First, the possible mechanisms for altering the heat transfer rates in the channels are: (i) increase in heat transfer due to the increased surface area, (ii) increase in the local heat transfer coefficient due to locally accelerated flow around the obstruction region and (iii) reduction in heat transfer due to the presence of recirculating zones. Recirculating zones reduce the heat transfer as the heat transfer mechanism in these regions is conduction dominated. Therefore, the total effect of multiple obstructions on heat transfer is a combination of all the above mechanisms. The heat transfer in the obstructed channels increases or decreases depending on the cumulative effect of the above three mechanisms. The increase in the surface area due to the obstructions is the same, in both geometries I and II. This means more heat transfer in both the cases due to mechanism (i). From the velocity field, the velocity around the tip of the obstructions in geometry II was observed to be higher than the corresponding velocity in geometry I. This means higher local heat transfer due to the accelerated flow near the obstructions in geometry II as compared to geometry I [mechanism (ii)]. Considering only these two mechanisms, average Nusselt numbers of geometry II need to be higher than those of geometry I. But, the average Nusselt numbers of geometry II are observed to be lower than those of geometry I. This is because of the predominant effect of mechanism (iii) in geometry II. That is, the recirculating flow regions substantially reduce the total heat transfer rate for this geometry.

Geometries III and IV ($Ar = 0.3$) were studied to investigate the effect of the channel aspect ratio on heat transfer by keeping the location and size of the obstructions as before (i.e. as in geometries I and II). The computed streamlines and isotherms for geometries III and IV were observed to be qualitatively similar in pattern to those of geometry I and geometry II respectively. Observations (a)–(e), as discussed earlier, were also found to be valid for these two geometries.

For all the above cases, it can be said that at high Rayleigh numbers, a boundary layer is formed on each plate. This is similar to the thermal behavior of a smooth channel at high Rayleigh numbers. In other words, the two walls of the channel become thermally independent of each other. The computed average Nusselt numbers for both the obstructed and smooth channels (with $Ar = 0.3$) were compared and a similar trend to that of Fig. 5 was observed. It is observed in this research that the average Nusselt number of either the obstructed or unobstructed channel increases with the aspect ratio. This is because of the definition of the Nusselt number used in this study [23]. Here, the Nusselt number is directly proportional to the channel width, b. Therefore, as the aspect ratio ($= b/L$) is increased by increasing b, the Nusselt number also increases.

As before, the percent reduction in local Nusselt number due to the presence of obstructions was determined for geometries III and IV. It was observed that the reduction in heat transfer at low Rayleigh numbers was more than the corresponding reduction at high Rayleigh numbers. The maximum reduction in heat transfer for geometry III was approximately 8.5% at $Ra = 5 \times 10^2$ and the minimum reduction in heat transfer was approximately 3% at $Ra = 10^4$. The maximum reduction for geometry IV was roughly 11% at $Ra = 5 \times 10^2$ and the minimum reduction was nearly 4% at $Ra = 2 \times 10^4$.

To study the effect of aspect ratio on the heat transfer rate, the average Nusselt numbers of all the four geometries are plotted in Fig. 6. From this figure, it can be clearly seen that the effect of aspect ratio decreases as Rayleigh number increases. At a Rayleigh

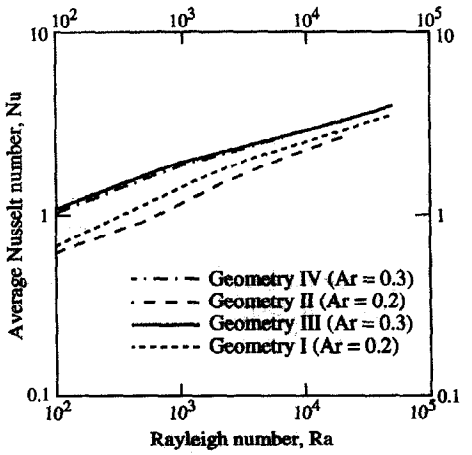

Fig. 6. Effect of aspect ratio on the rate of heat transfer for obstructed channels.

number of 10^2, there is a difference of nearly 61% in the average Nusselt numbers between geometries I ($Ar = 0.2$) and III ($Ar = 0.3$). This percentage difference decreased with increasing Rayleigh number, with the lowest difference being 13% at $Ra = 5 \times 10^4$. Similarly, the maximum difference between geometries II ($Ar = 0.2$) and IV ($Ar = 0.3$) is approximately 72% at $Ra = 10^2$ and the minimum difference is 22% at $Ra = 2 \times 10^4$. The percentage difference decreased with increasing Rayleigh number. These numerical values suggest that for the same type of geometry, the gap between the two curves corresponding to two aspect ratios narrows down as Ra increases. Here, the same type of geometry means that either the obstructions are facing each other or are separated by a fixed distance. This effect of the aspect ratio can be understood by examining the nondimensional governing equation. It can be seen from the nondimensional energy equation that the term with which aspect ratio multiplies (e.g. the conduction term in the streamwise y direction), is expected to be relatively small. On the other hand, at lower values of Rayleigh number, the flow approaches a fully developed channel flow. This mechanism increases the effect of aspect ratio at low values of Rayleigh number.

5. CONCLUSIONS

From the present study for channels with obstructions on both walls, several conclusions can be drawn. These are discussed next. The average Nusselt number and mass flow rate increase as the Rayleigh number increases. The velocities at the tips of the obstructions at $Ra = 10^4$ are compared in all the cases. It is found that for the same Rayleigh number, the velocity is more for the geometries II and IV (obstructions facing each other) as compared to the geometries I and III. The computed average Nusselt numbers of the obstructed channel are compared with those of the smooth channel. It is found that the average Nusselt numbers for obstructed channels are less than those of the smooth channels. Thus, the presence of the obstructions reduces the heat transfer. Local Nusselt number is maximum at the entrance of the channel. In the case of the obstructed walls, it can be said that (a) initially, the local Nusselt number decreases from the channel entrance to the lower intersection of obstruction with the wall, (b) then reaches a peak value at the lower, outer corner or tip of the obstruction and (c) then decreases up to the upper intersection of the obstruction with the wall. The effect of the aspect ratio decreases as the Rayleigh number increases. At any particular Rayleigh number, the percentage reduction is more for geometry II than geometry I. The maximum reduction in heat transfer for geometry II is approximately 31% and occurred at $Ra = 5 \times 10^2$. The minimum reduction in heat transfer is approximately 7.5% and occurred at $Ra = 2 \times 10^4$. The maximum reduction in heat transfer for geometry III is roughly 8.5% at $Ra = 5 \times 10^2$ and the minimum reduction is 3% at $Ra = 10^4$.

REFERENCES

1. S. W. Churchill, A comprehensive correlating equation for buoyancy induced flow in channels, *Lett. Heat Mass Transfer* **4,** 193–199 (1977).
2. A. Bar-Cohen and W. M. Rohsenow, Thermally optimum spacing of vertical, natural convection cooled, parallel plates, *J. Heat Transfer* **106,** 116–123 (1984).
3. E. M. Sparrow and P. A. Bahrami, Experiments on natural convection from vertical parallel plates with either open or closed edges, *J. Heat Transfer* **102,** 221–227 (1980).
4. W. Aung, K. I. Beith and T. J. Kessler, Natural convection cooling of electronic cabinets containing arrays of vertical circuit cards, ASME Paper No. 72-WA/HT-40, presented at the ASME Winter Annual Meeting, New York, pp. 26–30 (1972).
5. N. K. Anand, Kim, S. H. Kim and L. S. Fletcher, The effect of plate spacing on free convection between heated parallel plates. In *Thermal Modeling and Design of Electronic Systems and Devices*, ASME HTD-Vol. 153, pp. 81–87 (1990).
6. E. K. Levy, Optimum plate spacings for laminar natural convection heat transfer from parallel vertical isothermal flat plates, *J. Heat Transfer* **93,** 463–465 (1971).
7. E. K. Levy, P. A. Eichen, W. R. Cintani and R. R. Shaw, Optimum plate spacings for laminar natural convection heat transfer from parallel vertical isothermal flat plates: experimental verification, *J. Heat Transfer* **97,** 474–476 (1975).
8. R. A. Wirtz and R. J. Stutzman, Experiments on natural convection between vertical plates with symmetric heating, *J. Heat Transfer* **104,** 501–507 (1982).
9. W. Aung, Fully developed laminar free convection between vertical plates heated asymmetrically, *Int. J. Heat Mass Transfer* **15,** 1577–1580 (1972).
10. W. Aung, L. S. Fletcher and V. Sernas, Developing laminar free convection between vertical flat plates with asymmetric heating, *Int. J. Heat Mass Transfer* **15,** 2293–2328 (1972).
11. B. W. Webb and D. P. Hill, High Rayleigh number laminar natural convection in an asymmetrically heated vertical channel, *J. Heat Transfer* **111,** 649–656 (1989).
12. J. R. Carpenter, D. G. Briggs and V. Sernas, Combined radiation and developing laminar free convection between vertical flat plates with asymmetric heating, *J. Heat Transfer* **98,** 95–100 (1976).
13. W. Cha, J. R. Lloyd and K. T. Yang, Numerical study of natural convection between two vertical parallel plates with one oscillating surface temperature. In *Numerical Simulation of Convection in Electronic Equipment Cooling*, ASME HTD-Vol. 121, pp. 31–38 (1989).
14. W. Kim, and R. F. Boehm, Combined free and forced convective heat transfer from multiple rectangular wall blocks in vertical channels. In *Mixed Convection And Environmental Flows*, ASME HTD-Vol. 152, pp. 1–8 (1990).
15. S. Habchi, and S. Acharya, Laminar mixed convection in a partially blocked, vertical channel, *Int. J. Heat Mass Transfer* **29,** 1711–1722 (1986).
16. S. A. M. Said, and R. J. Krane, An analytical and experimental investigation of natural convection heat transfer in vertical channels with a single obstruction, *Int. J. Heat Mass Transfer* **33,** 1121–1134 (1990).
17. S. A. M. Said, and A. Muhanna, Investigation of natural convection in a vertical parallel-walled channel with a single square obstruction. In *Simulation And Numerical Methods in Heat Transfer*, ASME HTD-Vol. 153, pp. 73–80 (1990).
18. A. Mehrotra and S. Acharya, Natural convection heat

transfer in smooth and ribbed vertical channels, *Int. J. Heat Mass Transfer* **36,** 236–241 (1993).
19. D. K. Gartling, *NACHOS* II—*a Finite Element Computer Program for Incompressible Flow Problems*—I. *Theoretical Background,* SAND86-1816, UC-32. Sandia National Laboratories, Albuquerque, NM (1987).
20. D. K. Gartling, *NACHOS* II—*a Finite Element Computer Program for Incompressible Flow Problems*—II. *User's Manual,* SAND86-1817, UC-32. Sandia National Laboratories, Albuquerque, NM (1987).
21. Z. Y. Zhong, K. T. Yang and J. R. Lloyd, Variable property effects in laminar natural convection in a square enclosure, *J. Heat Transfer* **107,** 133–138 (1985).
22. E. M. Sparrow and J. L. Gregg, The variable fluid property problem in free convection, *J. Heat Transfer* **80,** 879–886 (1958).
23. P. Viswatmula, Free convection flows in vertical channels with two rectangular obstructions on opposite walls, M. S. Thesis, Montana State University (1993).